

A Theoretical Study of Acoustic Glitches in Low-Mass Main-Sequence Stars

Kuldeep Verma, H. M. Antia

Tata Institute of Fundamental Research, Homi Bhabha Road, Mumbai 400005, India

`kuldeepv@tifr.res.in`, `antia@tifr.res.in`

and

Sarbani Basu

Department of Astronomy, Yale University, P. O. Box 208101, New Haven CT 06520-8101,
U.S.A.

`sarbani.basu@yale.edu`

and

Anwesh Mazumdar

Homi Bhabha Centre for Science Education, Tata Institute of Fundamental Research, V.
N. Purav Marg, Mankhurd, Mumbai 400088, India

`anwesh@tifr.res.in`

Received _____; accepted _____

ABSTRACT

There are regions in stars, such as ionization zones and the interface between radiative and convective regions, that cause a localized sharp variation in the sound speed. These are known as “acoustic glitches”. Acoustic glitches leave their signatures on the oscillation frequencies of stars, and hence these signature can be used as diagnostics of these regions. In particular, the signature of these glitches can be used as diagnostics of the position of the second helium ionization zone and that of the base of the envelope convection zone. With the help of stellar models we study the properties of these acoustic glitches in main-sequence stars. We find that the acoustic glitch due to the helium ionization zone does not correspond to the dip in the adiabatic index Γ_1 caused by the ionization of HeII, but to the peak in Γ_1 between the HeI and HeII ionization zones. We find that it is easiest to study the acoustic glitch due to the helium ionization zone in stars with masses in the range $0.9\text{--}1.2 M_\odot$.

Subject headings: stars: interiors; stars: oscillations; stars: main-sequence

1. Introduction

It is known that a steep variation in the sound speed or its derivatives inside a star introduces an oscillatory component, $\delta\nu$, in the frequencies of stellar oscillations as a function of the radial order of the eigenmodes (Gough & Thompson 1988; Vorontsov 1988; Gough 1990), which is proportional to $\sin(4\pi\tau_g\nu_{n,l} + \phi)$, where n , l , $\nu_{n,l}$, and τ_g are respectively the radial order, the degree, the eigenfrequency, and the acoustic depth (i.e., sound travel time) of the sharp feature as measured from the stellar surface. These variations arise in a number of regions such as the discontinuity in the second derivative of the sound speed at the boundaries of the convection zones as well as the localized depressions in the adiabatic index Γ_1 in the ionization zones of abundant elements.

The important ionization zones when it comes to acoustic glitches are those where HI, HeI, or HeII undergo ionization. Of these, the HI ionization zone is very broad and the signal gets damped very quickly — the amplitude of the signal is proportional to $e^{-8\pi^2\Delta^2\nu^2}$ (Houdek & Gough 2007) with Δ being the half-width (σ) of a Gaussian profile that approximates the depression of Γ_1 in HI ionization zone. A typical value of Δ for main-sequence stars considered in this work is about 150 s (Houdek & Gough 2007) implying that the amplitude will reduce by a factor of e at a frequency of around 700 μHz . Furthermore, the acoustic depth of this signal is very small and therefore any left-over signal behaves like a smooth function of frequency which makes it difficult to determine its oscillatory nature. The HeI ionization zone overlaps with the HI ionization zone and is again difficult to isolate. Similarly, the boundary of convective cores cannot be detected because of aliasing (Mazumdar & Antia 2001). Thus in most cases only the HeII ionization zone and the base of the envelope convection zone (CZ) can be probed through acoustic glitches.

The acoustic glitches for several stars have been studied using data from *CoRoT*

and *Kepler* missions. Using *CoRoT* data, Miglio et al. (2010) determined the location of the second helium ionization zone for the red giant HR 7349, while Roxburgh (2011) and Mazumdar et al. (2011, 2012) determined the same for a solar type star HD 49933. Mazumdar et al. (2014) have used *Kepler* data to determine the depth of HeII ionization zone as well as the depth of the surface convection zone in 19 stars. Verma et al. (2014) have used *Kepler* data to estimate the helium abundance of a binary system, 16 Cyg A and B.

In this work we study the signal expected from the HeII ionization zone and from the base of the envelope convection zone in main-sequence stars with masses between $0.8M_{\odot}$ and $1.5M_{\odot}$ using stellar models. We have restricted the study to main-sequence stars since the presence of mixed modes in more evolved stars make it difficult to isolate the oscillatory signal reliably. The mass limits are determined by the strength of the He signal and whether or not we expect a star to have a deep enough envelope convection zone to excite oscillations. For stars at the subsolar mass end, the dip in Γ_1 caused by HeII ionization is rather shallow, and hence the amplitude of the oscillatory signal is very small. For stars of relatively high mass, greater than about $1.5M_{\odot}$, the convection zone becomes very shallow and overlaps with the HeII ionization zone making it difficult to fit the signal produced by the two glitches. Furthermore, the envelope convection zone may split into two parts in such stars introducing two additional convective boundaries in a narrow region, which complicates the effective signature from the base of the convection zone. In this work we use stellar models in an attempt to identify stars for which the oscillatory signal can be reliably used to study the stellar properties. The mass-range studied in this work is similar to Basu et al. (2004), who proposed that the acoustic glitches can be used to measure the helium abundance in the envelope of these stars. That work was aimed at using the amplitude of the HeII signal and did not pay much attention to the acoustic depth of the glitches. In particular, they did not attempt to identify the fitted acoustic depths of the

acoustic glitches to specific features in the stellar models. This issue was addressed to some extent by Houdek & Gough (2007) who found that inclusion of acoustic glitch from HeI ionization zone improves the agreement between the fitted acoustic depth of the glitch from HeII ionization zone and the actual acoustic depth of the HeII ionization zone in a solar model. In this work we wish to investigate this in more detail. Note that Broomhall et al. (2014) had a similar theoretical study for the acoustic depth of the HeII ionization zone in the red giant models.

There is often a systematic offset in the acoustic depths of the glitches obtained from fitting their signature in the frequencies with that calculated using the sound speed profile. A part of this offset is caused by the uncertainty in the definition of the effective surface of the star from which the acoustic depth is measured. Balmforth & Gough (1990) have argued that in the outer convection zone, the squared sound speed, c^2 , to some approximation decreases linearly with increase in radius. Hence, they suggested that the seismic surface can be defined as the layer at which the extrapolated c^2 vanishes. In a solar model the surface defined in this manner is located at an acoustic height of about 225 s above the photosphere. The uncertainty in the location of outer boundary affects the acoustic depths of all glitches by the same amount. For stellar models without overshoot, the location of acoustic glitch at the base of the convection zone is unambiguously defined — this is the point where the adiabatic temperature gradient in the convection zone changes to the radiative temperature gradient giving rise to a discontinuity in the second derivative of the sound speed. Hence we can use the fitted acoustic depth of the convection zone signal to estimate the location of the surface making it easy to compare the fitted acoustic depth of the glitches to the actual acoustic depth in a model. To avoid this uncertainty in definition of acoustic surface, Ballot et al. (2004) and Mazumdar (2005) have suggested that the acoustic radius be used instead. The acoustic radius of a glitch is the sound travel time from the center to the location of the glitch. However, the form of the fitting functions

involve the acoustic depths of the glitches, and therefore will have to be transformed to the acoustic radius using the total acoustic radius of the star. The stellar acoustic radius is related to the large frequency separation. But this is not devoid of uncertainties because of the contribution of the surface term to the frequencies and hence to the large separation. Thus it is not clear if this transformation would help, and hence we used acoustic depth in this work.

The issue of the uncertainty in the position of the glitch is a bit more complicated in the case of the He ionization zones. Unlike the convection-zone base, the ionization zones are merely regions of sharp change. They do not lead to a discontinuity in the derivatives of the adiabatic index, and hence, there is no discontinuity in the derivatives of the sound speed either. The depressions D1, D2, and D3 in Γ_1 , as shown in Fig. 1, due to HI, HeI, and HeII ionization zones respectively, result in a peak P2, which has a sharper profile than the depression due to the HeII ionization. It has generally been assumed that the acoustic glitch whose signature we see in the frequencies is caused by D3 where the bulk of HeII ionizes (Monteiro & Thompson 2005; Houdek & Gough 2007). However, the fitted acoustic depth of the signal does not match the acoustic depth of D3 (Houdek & Gough 2007; Mazumdar et al. 2014). Broomhall et al. (2014) found that for red giant models the fitted acoustic depth is close to that of P2. Thus it is worth investigating which feature in the He ionization zone results in the oscillatory signature, in particular, if it is the depression D3 as had always been assumed, or whether it is the peak P2. In this work we attempt to identify the location of the glitches by fitting the oscillatory signal to frequencies of stellar models and comparing the fitted value of τ_g with the acoustic depths of various features in the models.

The rest of the paper is organized as follows: Section 2 describes the techniques for fitting the oscillatory signal, Section 3 describes the set of stellar models constructed to

study the acoustic glitches, Section 4 describes the results, and Section 5 gives a summary of results.

2. The fitting techniques

We carried out the analysis using two different techniques to fit the oscillatory signal in the frequencies due to the major acoustic glitches as a function of the radial order, or equivalently, the frequency. The first technique fits directly the frequencies whereas the second fits their second differences. The details of the techniques are described below.

2.1. Fitting the frequencies directly (Method A)

We fitted the oscillation frequency, $\nu_{n,l}$, directly by modelling the smooth and the oscillatory components appropriately. For each degree l , the smooth component was modelled using a fourth degree polynomial in radial order n , and the form of the oscillatory signals arising from the base of convection zone and from the HeII ionization zone were adapted from Houdek & Gough (2007). The full expression fitted to the frequency is given by

$$f(n, l) = \sum_{i=0}^4 A_{l,i} n^i + \frac{A_c}{\nu^2} \sin(4\pi\tau_{\text{CZ}}\nu + \psi_{\text{CZ}}) + A_h \nu e^{-c_2\nu^2} \sin(4\pi\tau_{\text{He}}\nu + \psi_{\text{He}}), \quad (1)$$

where $A_{l,i}$ are the coefficients of the polynomial in n that defines the smooth component of the frequencies; A_c and A_h give a measure of the amplitudes of the CZ signal and the HeII signal respectively; c_2 is a parameter related to the thickness of the HeII ionization zone; τ_{CZ} and τ_{He} are respectively the acoustic depths of the CZ base and the HeII ionization zone respectively; ψ_{CZ} and ψ_{He} define the phases of the two oscillatory signals. The 4×5

elements of $A_{l,i}$ (assuming that we are fitting modes with degree l of 0–3) along with A_c , τ_{CZ} , ψ_{CZ} , A_h , c_2 , τ_{He} , ψ_{He} are 27 free parameters. The three terms in Eq. (1) are respectively the smooth component, signal from the base of convection zone, and signal from the HeII ionization zone. It is not possible to observe $l = 3$ modes in most stars, and therefore we use these modes only for the Sun and 16 Cyg A, for which they have been observed. 16 Cyg A is one of the best-studied stars using data from *Kepler* (Metcalf et al. 2012; Verma et al. 2014) and has largest number of modes after the Sun with a reasonably precise set of frequencies. For the rest of the models, we use only modes of $l = 0$ –2. Most of the results presented in this work are based on the fit to the above expression. We have also studied for the Sun and 16 Cyg A the possibility of separating out the oscillatory signal caused by the HeI ionization by adding one more oscillatory term similar to the HeII term to Eq. (1).

We fitted the frequencies to the function $f(n, l)$ using a nonlinear least-squares fit with second derivative smoothing. The smoothing, which is applied to only the first term in Eq. (1), provides additional constraints that enable us to determine a relatively large number of parameters. We used the same value of the smoothing parameter as in Verma et al. (2014). Since the nonlinear minimization may not converge to the global minimum for different starting guesses, we repeated the minimization with multiple sets of initial guesses (100 when fitting only the HeII and CZ signals, 500 when the HeI term is added) of the free parameters. The different sets of initial guesses were obtained by randomly perturbing a reasonable value for each parameter. The solution with the minimum among the set of χ^2 generated in these trials was accepted as the best fit to the data. In order to estimate the uncertainties on the fitted parameters, the fitting process was repeated for 1000 realizations of the data obtained by perturbing the frequencies with Gaussian random errors with standard deviation equal to the uncertainties in the frequencies. The uncertainties used depends on the star or model being fit and is discussed further in Section 4.

2.2. Fitting second differences (Method B)

In this technique, we enhanced the oscillatory signal by taking the second differences (Gough 1990; Basu et al. 1994, 2004; Mazumdar 2005) of the frequencies with respect to the radial order, n ,

$$\delta^2\nu_{n,l} = \nu_{n-1,l} - 2\nu_{n,l} + \nu_{n+1,l}. \quad (2)$$

The main advantage of taking second differences is that it removes the contribution from the dominant smooth trend which is a linear function of n . On the other hand, taking the second differences introduces correlations between neighboring points that need to be accounted for by using the covariance matrix while defining the χ^2 function. Another disadvantage of this technique is that the amplitude of oscillatory signal from small τ_g features is reduced significantly. We fitted the second differences to oscillatory signals from the base of the convection zone and the HeII ionization zone (Mazumdar & Antia 2001). We used the following form which has been adapted from Houdek & Gough (2007),

$$\begin{aligned} \delta^2\nu = & a_0 + a_1\nu + a_2\nu^2 + \frac{b_2}{\nu^2} \sin(4\pi\nu\tau_{CZ} + \phi_{CZ}) \\ & + c_0\nu e^{-c_2\nu^2} \sin(4\pi\nu\tau_{He} + \phi_{He}), \end{aligned} \quad (3)$$

where $a_0, a_1, a_2, b_2, c_0, c_2, \tau_{CZ}, \tau_{He}, \phi_{CZ}, \phi_{He}$ are 10 free parameters. The first three terms represent the smooth part of the function which remains after the second differences are calculated, the next term represents the contribution from the base of the convection zone with b_2 giving a measure of the amplitude of the signal, τ_{CZ} its acoustic depth, and ϕ_{CZ} the phase, while the last term represents the contribution from the HeII ionization zone with c_2 related to the thickness of the ionization zone, c_0 giving a measure of the amplitude of the signal, τ_{He} its acoustic depth, and ϕ_{He} the phase. The number of terms needed to approximate the smooth part depends on the range of frequencies that are observed and the errors in these frequencies. Since in this case we are mainly dealing with model frequencies, we use the observed solar frequencies to decide the number of terms needed.

Adding more terms doesn't lead to a statistically significant reduction in χ^2 . Since this method uses fewer parameters as compared to Method A, in some cases the fit is not as good as that for Method A. This is particularly the case when the frequency range used is large and the errors in frequencies are small, as is the case for the Sun and for frequencies of stellar models. An important difference between the two methods is that in Method B, the smooth part is independent of l , which may be justified because a large part of the smooth trend gets filtered out when second differences are taken. But in some cases a residual l dependence may remain in the second differences also. We also repeated the exercise after including an additional term for HeI ionization zone for the Sun and 16 Cyg A, as was done in Method A.

The parameters in Eq. (3) were determined using a nonlinear least-squares fit, with χ^2 defined using the covariance matrix. The covariance matrix was calculated by assuming that the errors in individual frequencies are not correlated. This is the usual approximation when using solar and stellar frequencies. Although, all frequencies are determined by using a single oscillation power spectrum, the frequencies are reasonably well separated and the correlation between frequencies of two different modes is quite small. If the covariance matrix for the observed frequencies is available it can be easily taken into account while calculating the error covariance matrix for the second differences. As in Method A, we made multiple (100/500) attempts to fit the signal using different initial guesses for the free parameters, which were obtained by randomly perturbing a reasonable value of the initial guesses. The minimum of the set of χ^2 obtained over these multiple attempts was chosen to be the best fit. Similarly, the errors in the fitted parameters were estimated by repeating the whole process for 1000 realizations of data obtained by randomly perturbing the frequencies.

3. Stellar models Used

The models were constructed using the evolutionary code MESA (Paxton et al. 2011). We used OPAL equation of state (Rogers & Nayfonov 2002), OP high temperature opacities (Badnell et al. 2005; Seaton 2005) supplemented with low temperature opacities from Ferguson et al. (2005). The metallicity mixture of Grevesse & Sauval (1998) was used. We used the reaction rates from NACRE (Angulo et al. 1999) for all reactions except $^{14}\text{N}(p,\gamma)^{15}\text{O}$ and $^{12}\text{C}(\alpha,\gamma)^{16}\text{O}$, for which updated reaction rates from Imbriani et al. (2005) and Kunz et al. (2002) were used. Convection was modelled using the standard mixing length theory (Cox & Giuli 1968) without overshoot, and diffusion of helium and heavy elements was incorporated using the prescription of Thoul et al. (1994).

We constructed models with an initial helium abundance of $Y_i = 0.28$, initial heavy element abundance of $Z_i = 0.02$, and mixing length parameter $\alpha = 1.91$ as obtained from solar calibration. The models cover a range in mass and age. The envelope helium and heavy element abundance get depleted for models of mass greater than $1.4M_{\odot}$ because of diffusion, therefore for these masses we use models without diffusion. In these cases we use a mixing-length parameter of $\alpha = 1.84$ as is obtained for a calibrated solar model without diffusion. Fig. 2 shows the evolutionary stages of the models in the H-R diagram.

In addition to these evolutionary sequences, we also constructed one solar model and a representative model for the solar analog 16 Cyg A. The 16 Cyg A representative model was constructed with a mass of $1.05M_{\odot}$, an initial helium abundance of 0.29, initial heavy element abundance 0.022, and age 6.9 Gyr.

4. Results

Before looking at models of other stars where there could be uncertainties in radius and luminosity, we first examined what happens if we compare results from a solar model and the Sun. Since the mass, radius, and luminosity of the Sun are known independently, solar models have the same radius and luminosity as the Sun. We also fitted the frequencies of 16 Cyg A and its model.

The uncertainties in the input frequencies affect the nature of the fits and determine the uncertainties in the fitted parameters. To estimate this uncertainty, we repeated the fitting process for each star/model for 1000 realizations of the data obtained by perturbing the frequencies with Gaussian random error with standard deviation equal to the quoted error-bars/weights on the frequencies. Since the evolutionary sequence of models are generic models and not those of any particular star with observed frequency estimate, there is no statistical uncertainty in the frequencies and the fitted parameters. However, we assumed that the frequencies of the models of the Sun and 16 Cyg A have the same weights as the corresponding observed frequency estimate. This was done to avoid systematic errors in the fitting. For other stellar models we assume an error of $0.1 \mu\text{Hz}$ in all modes, which is a reasonable estimate of the uncertainties in the asteroseismic data, and therefore gives an idea of the precision to which we can determine the glitch parameters of a real star.

4.1. Results for the Sun and 16 Cyg A

We used the solar data set obtained by the Birmingham Solar Oscillation Network (BiSON; Elsworth et al. 1991) listed in Table 1 of Chaplin et al. (2007). The frequencies of 16 Cyg A were those obtained by NASA’s *Kepler* mission and listed in Table 2 of Verma et al. (2014). Verner et al. (2006) had shown that it is possible to determine the

signature of acoustic glitches in low-degree modes obtained by BiSON if the data covers an interval of 6 months or longer, and thus we were confident that we would be able to fit the signatures of the acoustic glitch in the frequencies obtained from a much longer time-series. We also fitted the frequencies of models of the Sun and 16 Cyg A. We determined the parameters in Eqs. (1) and (3) using the techniques described in Section 2. The modes of degree 0, 1, 2, and 3 were used in the fits for the Sun (total 72 modes in the frequency range of 1.4-4.0 mHz) and 16 Cyg A (total 53 modes in the frequency range of 1.3-2.9 mHz).

4.1.1. *Fitting only the HeII and CZ signals*

The fits to the BiSON data are shown in Fig. 3. The left panel of Fig. 3 shows the result of fitting Eq. (1) to the observed frequencies using Method A. To see the oscillatory component, $\delta\nu$, clearly, we subtracted the smooth component fitted by the polynomial in Eq. (1). The lower panel shows the normalized residuals of the fit obtained by dividing the residual of the fit by the error in the frequency. Note the significantly large residual and the oscillatory trend in it. This could be due to inaccurate modelling of the oscillatory signal, and will be explored later. The fitted parameters obtained using Methods A and B are listed in Table 1 for both the Sun and a solar model. In the table, χ^2 denotes the weighted least-squares residual of the fit, A_{CZ} and A_{He} denote respectively the amplitude of CZ and He signal averaged over the frequency range used in the fit, and Δ_{He} denotes the half-width of the glitch as obtained using fitting parameter c_2 of Eqs. (1) and (3) ($\Delta_{He} = \sqrt{c_2/8\pi^2}$). The amplitudes of the signals obtained by fitting the second differences in Method B have been converted to the amplitude of the signal in the frequencies by dividing the second-difference amplitudes by $4\sin^2(2\pi\tau_g\Delta_0)$, where Δ_0 is the large frequency separation (Houdek & Gough 2007).

From Table 1 we can see that the fitted τ_{He} and τ_{CZ} for the solar model and the Sun

are in close agreement with each other with the difference being about 1%. However, in the case of the solar model we find that the fitted value of τ_{CZ} is larger than the acoustic depth of the base of convection zone (2244 s) as measured from the top of the atmosphere at an optical depth of 10^{-5} . This difference can be attributed to the choice of the stellar surface and by extending the model further by about 400 km it is possible to match the two values. We find that if the model is extended to an optical depth of 2×10^{-6} , the fit does not change much, for example the fitted τ_{CZ} using Method A is 2294 ± 5 s, while the calculated acoustic depth is 2301 s. Clearly both of them are now in good agreement with each other. The issue is different with τ_{He} . The fitted value of τ_{He} is smaller than the calculated acoustic depth of the HeII ionization zone defined as the minimum in Γ_1 (D3 in Fig. 1), the calculated acoustic depth of this dip is $\tau_{D3} = 764$ s. The fitted value is in fact close to the acoustic depth of a layer above the HeII ionization zone where Γ_1 is maximum (P2 in Fig. 1) which has a calculated acoustic depth of $\tau_{P2} = 668$ s. Extending the stellar atmosphere upwards further increases the acoustic distance between the fitted τ_{He} and τ_{D3} , while the fitted τ_{He} remains consistent with τ_{P2} .

We repeated the same exercise as above for 16 Cyg A and the results are listed in Table 1. The table also shows the results for a representative stellar model for this star. Similar to the solar model, the results for the model of 16 Cyg A also shows that the fitted τ_{He} is closer to the acoustic depth of point P2 (911 s) rather than D3 (1051 s).

4.1.2. *Fitting the signal from HeI ionization zone explicitly*

Houdek & Gough (2007) have argued that there should be an oscillatory contribution to the frequency from HeI ionization zone too; however, it is not clear whether the contribution is significant and detectable since the HeI ionization zone overlaps with HI ionization zone. The residuals shown at the bottom of the left panel of Fig. 3 seem to have

an oscillatory signal of period about 500 μHz , which corresponds to a glitch at an acoustic depth of 1000 s. This acoustic depth does not correspond to the (shallow) HeI ionization zone, but to a layer just *below* the HeII ionization zone where Γ_1 is close to its asymptotic value of 5/3 (see Fig. 1).

To study the effect of the HeI ionization zone we included one more term, similar to the last term, in Eq. (1) resulting in four additional parameters. Two mathematically similar terms usually destabilize a fit, and hence, to stabilize the fit we fixed the ratio of the acoustic depths of HeI and HeII ionization zones ($\eta \equiv \tau_I/\tau_{II}$) and keep the other three parameters free. This differs from the methodology of Houdek & Gough (2007) who fixed all four parameters using theoretically expected ratios between the parameters of the HeI and HeII signals. We varied the ratio η in the range 0.2–0.9 and obtained the best fit to the data for each value of η . The fitted parameters obtained using Method A for the solar model and the BiSON frequencies are listed in Table 2 for different values of η . Clearly the two helium-glitch model improves the fit with χ^2 reducing significantly compared to those in the Table 1. However, the χ^2 has a minimum at around $\eta = 0.25$, and the corresponding fit to the observed frequencies is shown in the right panel of Fig. 3. Since Method A fits the smooth and oscillatory components of frequency together, the addition of the second helium-glitch changes the smooth component as well. As a result, the oscillatory signal $\delta\nu$ obtained by subtracting the smooth part of frequency, looks very different in the two panels. The fit corresponds to the helium-glitches at acoustic depths of 172 s and 689 s for the observed frequencies, and at 170 s and 678 s for the solar model. These acoustic depths do not correspond to the HeI and HeII ionization zones, instead, one of them again corresponds to the peak P2 in Γ_1 profile and the other corresponds to a peak P1 near the surface (see Fig. 1). Note that the fitted values of both, τ_{He} and the amplitude of the He signal, approaches that obtained in Table 1 as η approaches 0.25 where χ^2 is minimum. For smaller value of η , the χ^2 of the fit increases, the fit becomes unstable, and it is difficult to

determine the value of any particular parameter reliably.

It may be noted that in the solar atmospheric model constructed with the MESA code, the temperature asymptotically approaches a constant value and hydrogen is not ionized. On the other hand, the temperature increases with height beyond the temperature minimum in the Sun, and hydrogen gets ionized once again, giving another dip in Γ_1 in the atmosphere, which results in the peak P1. Fig. 4 shows the Γ_1 profile in a solar model where the atmospheric model of Vernazza et al. (1981) is added at the top. In this atmospheric model the temperature increases beyond a height of about 500 km and HI gets ionized giving another dip in Γ_1 .

The above analysis suggests that the total frequency of a solar-like star can effectively be written as, $\nu = \nu_s + \delta\nu_I + \delta\nu_{II} + \delta\nu_{CZ}$, where ν_s is the smooth part of the frequency coming from the smooth profile of Γ_1 as shown by the dotted line in Fig. 4, $\delta\nu_I$ and $\delta\nu_{II}$ are the contribution of the peaks on top of the dotted line, and $\delta\nu_{CZ}$ is the contribution of the glitch at the base of the convection zone.

Similar results were obtained by fitting the second differences using Method B. In this case, the χ^2 is much larger and the reduction on adding the HeI term is rather modest, but χ^2 still decreases with η . For the solar model, χ^2 decreases from a value of 1124 when the HeI term is not included to 988 for $\eta = 0.8$ and to 976 for $\eta = 0.2$. Similarly, for the observed frequencies the χ^2 reduces from a value of 1080 without HeI term to 1009 for $\eta = 0.8$ and 1001 for $\eta = 0.2$. This behavior may be expected since taking the second difference modifies the amplitude of the oscillatory signal by a factor of $4 \sin^2(2\pi\tau_g\Delta_0)$, where τ_g is the acoustic depth of the glitch and Δ_0 is the large frequency separation. This factor is 1.23 for the HeII signal, while it reduces to 0.82, 0.48, 0.22 and 0.06 for the HeI signal when $\eta = 0.8, 0.6, 0.4$ and 0.2 respectively. However, the errorbars in the second differences increase by about a factor of 2.5 as compared to those in the frequencies. As a

result, this method is not effective in detecting the oscillatory signal from glitches at low acoustic depths and the improvement is not as great as in the case of Method A when additional term is included in the fit.

Since the acoustic depth of the near-surface glitch (from P1) is very small, if the frequency range included in the fit is not large enough to show the oscillatory signal, its contribution will appear as a smooth component of the frequency. This is particularly true if we do not have a sufficient number of low-frequency modes. To check whether we can detect the signal from the near-surface glitch for stars other than the Sun, we repeated the exercise above for 16 Cyg A using Method A, with and without the additional HeI term to see whether it improves the fit. Note from Table 1 the small values of the χ^2 for the model frequencies, which indicates that the one helium-glitch model is very close to the true model in the observed frequency range of this star. We found that the additional term does not improve the fit – the χ^2 does not reduce significantly irrespective of the value of η . For example, the χ^2 for the observed frequencies of 16 Cyg A reduces to 72.0 when $\eta = 0.25$. Similar results were found when we fitted the observed solar frequencies in a frequency range restricted by the radial orders of the available 16 Cyg A data. This suggests that the observed frequency range of 16 Cyg A is not large enough to detect the signal from the near-surface glitch.

4.1.3. Fitting the HeI signal using artificial model

To check if we can expect to detect the presence of the oscillatory signal from the HeI ionization zone at all, we constructed a solar model with artificially increased helium ionization potentials to 54 eV for HeI and 94 eV for HeII. This allows us to separate out the HI and HeI ionization zones. The Γ_1 profile for this model is shown in Fig. 5. To suppress the signal from P1, we exclude frequencies at the lower end and fit the signal in

the frequency range 1.9–4.0 mHz using Method A. A single helium-glitch model fits the oscillatory signal at $\tau_{\text{He}} = 687$ s with $\chi^2 = 47.1$. The fitted τ_{He} in this case is closer to the peak P2 between the HI and the HeI zones as that peak is sharper than the peak P3. Including an additional oscillatory term as above reduced the χ^2 to 10.6 at $\eta = 0.65$. In other words, we definitely fit signals from both the HeI and HeII ionization zones, i.e., if the HI and HeI ionization zones are separate, we can isolate the HeI signature. The fitted acoustic depths were found to be 620 s and 949 s, both of which correspond to the peaks in Γ_1 just above the respective ionization zones (labelled as P2 and P3 in Fig. 5). Thus it is clear that for the cases considered thus far the fitted acoustic depths τ_{He} correspond to the peaks in Γ_1 above the ionization zones and not the dips in Γ_1 caused by the process of ionization. Similar result was found by Broomhall et al. (2014) for red giant stars.

In the limited frequency range that is observed for stars other than the Sun, the contribution of the near-surface glitch cannot be separated from the smooth component of the frequency, and is thus difficult to fit. However it may be noted from Tables 1 and 2 that the parameters of the glitch between HeI and HeII ionization zone do not depend on whether one helium-glitch model is fitted or two helium-glitch model with $\eta = 0.25$ is fitted. Therefore, we can reliably study the properties of the peak in the Γ_1 -profile (P2 in Fig. 4) by fitting the frequencies to a single glitch from ionization zones. Hence all results in the next subsection are obtained using such fits. It may be noted that this single glitch corresponds to the peak between the HeI and HeII ionization zones and hence we refer to it as “due to He ionization zones”.

4.2. The He and CZ signals of other main-sequence models

We fitted the frequencies, and the second differences of frequencies, of all the models described in Section 3 to Eqs. (1) and (3). The fits used 48 modes around the

frequency of maximum power, ν_{\max} , which was calculated using the usual scaling relation (Kjeldsen & Bedding 1995). We used only low-degree modes $l = 0, 1, 2$ that we expect to observe on most stars. As mentioned earlier, we assumed a nominal uncertainty of $0.1 \mu\text{Hz}$ for each mode for the purpose of defining the weights in the fits.

Fig. 6 shows the fitted average amplitude of He and CZ signal as a function of effective temperature (T_{eff}) and logarithm of the surface gravity ($\log g$). The amplitude of He signal increases with effective temperature. The change with $\log g$ at higher masses is a reflection of the change in T_{eff} as the star evolves. It may be noted that the models of mass $1.4M_{\odot}$ and $1.5M_{\odot}$ were constructed without diffusion, and therefore are physically different from the rest of the models and fall slightly off the trend in the figure. For a star of given mass and/or effective temperature, the amplitude of signal due to He ionization zone depends on the amount of helium present there, hence it can be used to determine the helium abundance (Basu et al. 2004; Monteiro & Thompson 2005; Verma et al. 2014). To determine the helium abundance, the amplitude of the helium signal can be calibrated with the models of similar mass and effective temperature with different helium abundance to estimate the current envelope helium abundance of the star. The amplitude of CZ signal seems to have a minimum around $T_{\text{eff}} = 6000 \text{ K}$. The increase in amplitude as T_{eff} reduces is quite modest, but for higher values of T_{eff} the amplitude increases more rapidly.

Fig. 7 shows the Γ_1 profiles for typical stellar models of mass $0.8M_{\odot}$ and $1.5M_{\odot}$ with roughly the same helium abundance. It can be seen that for low mass stars the dip in Γ_1 due to HeII ionization zone is very shallow, which reflects in the small amplitude of the oscillatory signal and can be fitted only if low frequency modes are included. The small peak around $\tau_g = 180 \text{ s}$ is due to the transition between the interior and the atmospheric model in the stellar model. Models with lower masses have even shallower dips making their signal almost impossible to fit. For $1.5M_{\odot}$ stellar model the dip in Γ_1 due to HeII

ionization zone is very pronounced and even the kink due to HeI ionization zone is visible. But the fits for higher mass stellar models are difficult because the HeII ionization zone and the base of the convection zone are relatively close, confusing their signal. Furthermore, these stars have large composition gradient at the boundary of the shrinking convective core, which results in a strong peak in the Brunt-Väisälä frequency, N . This introduces additional effects that are not modelled by the fitting function used. Similar peaks in the Brunt-Väisälä frequency may also be seen in the lower mass stars at the end of their main-sequence life due to large composition gradient in the core.

Fig. 8 shows N as a function of radius for a few models with masses of $1.1M_{\odot}$ and $1.3M_{\odot}$. We had no difficulty in fitting the signal of the He ionization zones for the $1.1M_{\odot}$ stellar models with age less than about 5.3 Gyr, and at these ages, the peak in N is less than about half of the lowest frequency used in the fits. As age increase, the peak in N increases, and we also find the quality of the fit deteriorates (as manifest in an increased χ^2 and uncertainties in the fitted parameters) even though the fits are done using model frequencies. A similar behavior is seen for models of mass less than $1.1M_{\odot}$, i.e., the fit becomes poor only very late along the main-sequence, close to the turnoff. The scenario is different for models of mass greater than $1.1M_{\odot}$ because these have convective cores. Most of the models of mass $1.3M_{\odot}$ show a strong peak in N just outside the convective core, which affects the frequencies in a manner that is not modelled by the asymptotic theory of stellar oscillations. We can see from Fig. 8 that all the models except the model with age 0.25 Gyr show a peak in N that is comparable to, or higher, than the lowest frequency used in the fitting. As a result, the smooth part of the frequency as a function of n becomes complicated for low frequency modes with frequencies comparable to the maximum of N in the core. This leads to difficulties in fitting the oscillatory signal caused by the acoustic glitches. These low frequency modes are crucial for fitting the He signal because its amplitude falls off rapidly with frequency, and hence removing these modes

from the fit is not a good option. The models shown in Fig. 8 were constructed without core overshoot. Inclusion of overshoot above the convective core will change the models, but it is not clear if that will reduce N just above the convective core substantially; the effect will depend on the prescription used to include overshoot. In the higher mass range, only a few models at the beginning of the main-sequence life do not have pronounced peak in N , but these are the models where the acoustic depths of HeII ionization zone and base of convection zone are similar, and hence, difficult to distinguish. Thus most models in this mass range are difficult to fit. Fits using Method B are affected more severely because it depends on calculating the second difference of the frequencies. It should, however, be noted that despite the difficulties in fitting the signal and the resulting large χ^2 , the fitted values of τ_{He} and τ_{CZ} are generally still reasonable (see Fig. 9), and thus it should be possible to infer these quantities from the observed frequencies for such stars if they are available. Mazumdar et al. (2014) also had difficulty in fitting oscillatory signal to observed frequencies for some stars, but found reasonable values of τ_{He} and τ_{CZ} for these stars.

The panels on the left-hand-side of Fig. 9 show the difference between the acoustic depth of the base of the convection zone and the fitted τ_{CZ} . The small offset that is seen can be attributed to the choice of the stellar surface. The red and blue points in the right-hand-side panels show the differences $\tau_{\text{P2}} - \tau_{\text{He}}$ and $\tau_{\text{D3}} - \tau_{\text{He}}$ respectively. Clearly, the peak marked P2 corresponds more closely to the fitted τ_{He} than the dip marked D3. We note from the figure, bearing in mind the offset due to the choice of the stellar surface, that the fitted τ_{He} for high mass stars correspond very closely to a layer near the peak marked P2, and this layer moves outwards for smaller masses. This is expected because the fitted τ_{He} is supposed to give the location of the peak in $\delta\Gamma_1$ and not in Γ_1 , where $\delta\Gamma_1$ is the difference between the actual Γ_1 and a smooth background profile that is similar to what is shown in Fig. 4 as the dotted line between D2 and D3. This dotted line has smaller slope for more massive stars than lower mass stars with a similar helium abundance. Hence, the

peak in $\delta\Gamma_1$ is close to the peak in Γ_1 , resulting in a good agreement between the fitted τ_{He} and τ_{P2} . The slope of the background line is larger for low mass stars thereby shifting the peak in $\delta\Gamma_1$ to a lower acoustic depth. We subtracted the background line for three models of mass $0.8M_\odot$, $1.0M_\odot$, and $1.5M_\odot$, and found the difference between the peak in Γ_1 and $\delta\Gamma_1$ to be 45 s, 30 s, and 15 s respectively. The difference between the blue and red points reflect the difference between the acoustic depth of P2 and D3.

5. Conclusions

In this work we have fitted oscillatory signal due to the He ionization zones and the base of the envelope convection zone for stellar models in the mass range of 0.8–1.5 M_\odot . We first studied the Sun, 16 Cyg A, and their representative models to investigate detecting a similar signal from the HeI ionization zone and to identify the fitted acoustic depths with known features in the stellar models. These stars were chosen as they represent the best case scenario for seismic studies. The technique was then applied to a series of stellar models.

We find that the fitted acoustic depth of the convection zone agrees with that in the stellar models, while the fitted acoustic depth of the He ionization zone corresponds to a layer above the HeII ionization zone where Γ_1 is close to maximum. Note that similar results were obtained by Broomhall et al. (2014) for models of red giants. This contradicts the common assumption that the signal of the acoustic glitch arises from the dip in Γ_1 caused by the HeII ionization and one that is used to derive the oscillatory contribution of the glitch from the asymptotic theory of stellar oscillations (Monteiro & Thompson 2005; Houdek & Gough 2007). The form of the oscillatory signal does not depend on whether it is due to a peak or a dip in Γ_1 as long as the glitch is approximately Gaussian in shape, and we can still use the same model to fit the oscillatory signal. However, we need to be

careful while interpreting the results to measure the depth of the ionization zones. We did not find any significant signal from the HeI ionization zone, but an attempt to fit the signal for a solar model yielded an additional glitch at $\tau_g \approx 170$ s, which is just above the HI ionization zone. Thus it appears that because of the overlap between ionization zones of HI and HeI, there is no peak in Γ_1 between the two and hence there is no clear oscillatory signal that can be fitted. This was further verified by constructing a solar model in which the ionization potentials of helium were increased to separate out the ionization zones. For that model the signal due to HeI ionization zone can be fitted successfully and the τ_g obtained from fitting the signature of the glitches in the oscillation frequencies corresponds to the peaks in the Γ_1 between the ionization zones.

The amplitude of the oscillatory signal caused by the He ionization zones increases with effective temperature and stellar mass. The signal is easiest to fit for masses between 0.9–1.2 M_\odot . For lower mass stars, the dip in Γ_1 in the HeII ionization zone is shallow and it is difficult to fit the signal reliably, unless low frequency modes are included. It may not be possible to observe these modes in the oscillation power spectrum of stars obtained from intensity measurements. For higher mass stars, the fit becomes unreliable because the acoustic depths of the two glitches ($\tau_{\text{He}}, \tau_{\text{CZ}}$) are very similar and hence difficult to fit. Another reason for difficulty in fitting the signal for high mass stars is the strong peak in the buoyancy frequency, N , just above the convective core. This causes frequencies of modes to deviate from the asymptotic approximation, thus distorting the smooth part of the frequency, which needs to be modelled appropriately to fit the signatures of the acoustic glitches. Similar difficulties arise even for low mass stellar models close to the end of their main-sequence life.

SB acknowledges partial support from NSF grant AST-1105930 and NASA grant NNX13AE70G. AM acknowledges support from the NIUS programme of HBCSE (TIFR).

REFERENCES

- Angulo, C., Arnould, M., Rayet, M., et al. 1999, *Nuclear Physics A*, 656, 3
- Badnell, N. R., Bautista, M. A., Butler, K., et al. 2005, *MNRAS*, 360, 458
- Ballot, J., Turck-Chièze, S., & García, R. A. 2004, *A&A*, 423, 1051
- Balmforth, N. J., & Gough, D. O. 1990, *ApJ*, 362, 256
- Basu, S., Antia, H. M., & Narasimha, D. 1994, *MNRAS*, 267, 209
- Basu, S., Mazumdar, A., Antia, H. M., & Demarque, P. 2004, *MNRAS*, 350, 277
- Broomhall, A.-M., Miglio, A., Montalbán, J., et al. 2014, *MNRAS*, 440, 1828
- Chaplin, W. J., Serenelli, A. M., Basu, S., Elsworth, Y., New, R., & Verner, G. A. 2007, *ApJ*, 670, 872
- Cox, J., & Giuli, R. 1968, *Principles of Stellar Structure: Physical principles*, *Principles of Stellar Structure No. v. 1* (Gordon and Breach)
- Elsworth, Y., Howe, R., Isaak, G. R., McLeod, C. P., & New, R., 1991, *MNRAS*, 251, 7P
- Ferguson, J. W., Alexander, D. R., Allard, F., et al. 2005, *ApJ*, 623, 585
- Gough, D. O. 1990, in *Lecture Notes in Physics*, Berlin Springer Verlag, Vol. 367, *Progress of Seismology of the Sun and Stars*, ed. Y. Osaki & H. Shibahashi, 283
- Gough, D. O., & Thompson, M. J. 1988, in *IAU Symposium*, Vol. 123, *Advances in Helio- and Asteroseismology*, ed. J. Christensen-Dalsgaard & S. Frandsen, 155
- Grevesse, N., & Sauval, A. J. 1998, *Space Sci. Rev.*, 85, 161
- Houdek, G., & Gough, D. O. 2007, *MNRAS*, 375, 861

- Imbriani, G., Costantini, H., Formicola, A., et al. 2005, *European Physical Journal A*, 25, 455
- Kjeldsen, H., & Bedding, T. R. 1995, *A&A*, 293, 87
- Kunz, R., Fey, M., Jaeger, M., et al. 2002, *ApJ*, 567, 643
- Mazumdar, A. 2005, *A&A*, 441, 1079
- Mazumdar, A., & Antia, H. M. 2001, *A&A*, 377, 192
- Mazumdar, A., Michel, E., Antia, H. M., & Deheuvels, S. 2011, in *Transiting Planets, Vibrating Stars and Their Connection*, ed. A. Baglin, M. Deleuil, E. Michel, C. Moutou, & T. Seaman, *Proceedings of Second CoRoT Symposium*, 197
- Mazumdar, A., Michel, E., Antia, H. M., & Deheuvels, S. 2012, *A&A*, 540, A31
- Mazumdar, A., Monteiro, M. J. P. F. G., Ballot, J., et al. 2014, *ApJ*, 782, 18
- Metcalf, T. S., Chaplin, W. J., Appourchaux, T. et al. 2012, *ApJ*, 748, L10.
- Miglio, A., Montalbán, J., Carrier, F., et al. 2010, *A&A*, 520, L6
- Monteiro, M. J. P. F. G., & Thompson, M. J. 2005, *MNRAS*, 361, 1187
- Paxton, B., Bildsten, L., Dotter, A., et al. 2011, *ApJS*, 192, 3
- Rogers, F. J., & Nayfonov, A. 2002, *ApJ*, 576, 1064
- Roxburgh, I. W. 2011, in *Transiting Planets, Vibrating Stars and Their Connection*, ed. A. Baglin, M. Deleuil, E. Michel, C. Moutou, & T. Seaman, *Proceedings of Second CoRoT Symposium*, 161
- Seaton, M. J. 2005, *MNRAS*, 362, L1

Thoul, A. A., Bahcall, J. N., & Loeb, A. 1994, *ApJ*, 421, 828

Verma, K., Faria, J. P., Antia, H. M., et al. 2014, *ApJ*, 790, 138

Vernazza, J. E., Avrett, E. H., & Loeser, R. 1981, *ApJS*, 45, 635

Verner, G. A., Chaplin, W. J., & Elsworth, Y. 2006, *ApJ*, 638, 440

Vorontsov, S. V. 1988, in *IAU Symposium, Vol. 123, Advances in Helio- and Asteroseismology*, ed. J. Christensen-Dalsgaard & S. Frandsen, 151

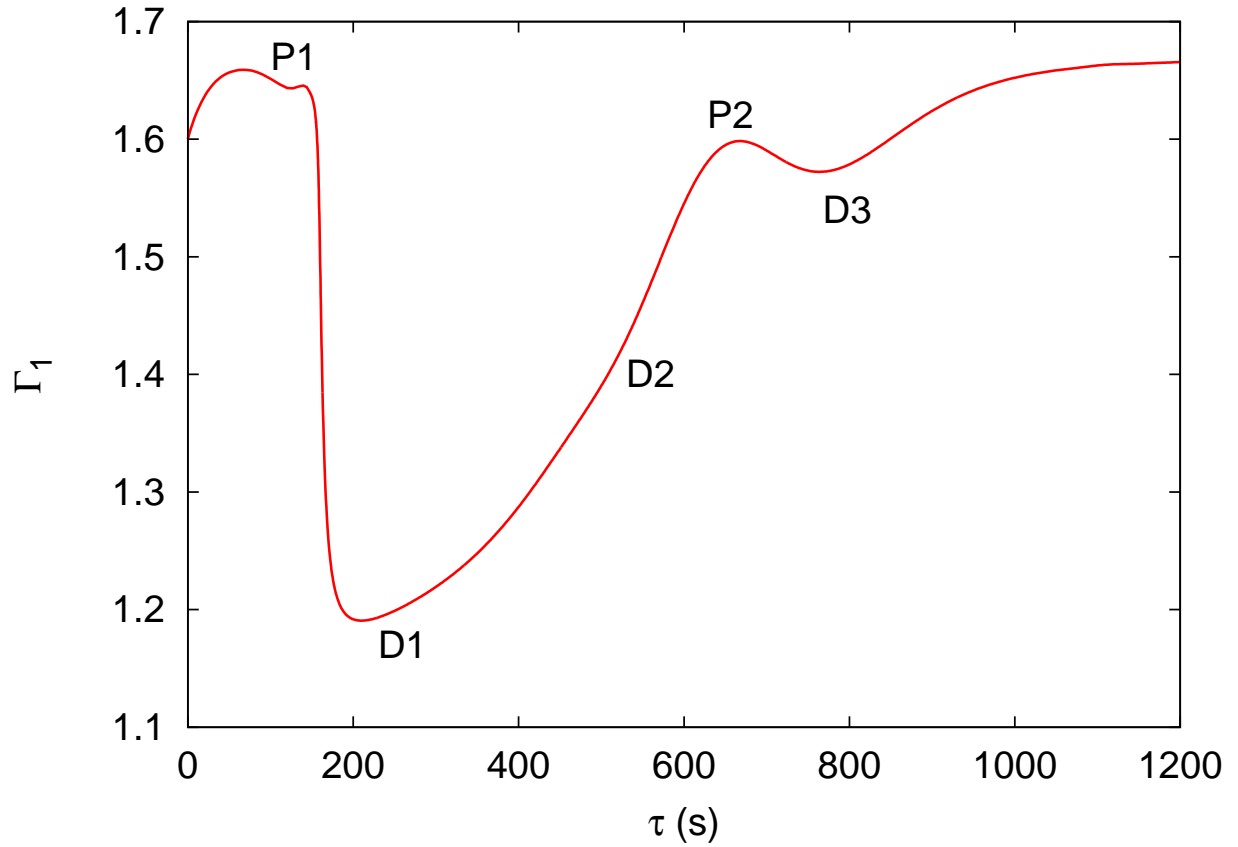


Fig. 1.— The first adiabatic index as a function of acoustic depth of a solar model. The labels D1, D2, and D3 refer to the hydrogen ionization zone, first helium ionization zone, and second helium ionization zone respectively, while P2 refers to peaks in Γ_1 that arise between the HeI and HeII ionization zones. On the other hand P1 is above the HI ionization zone.

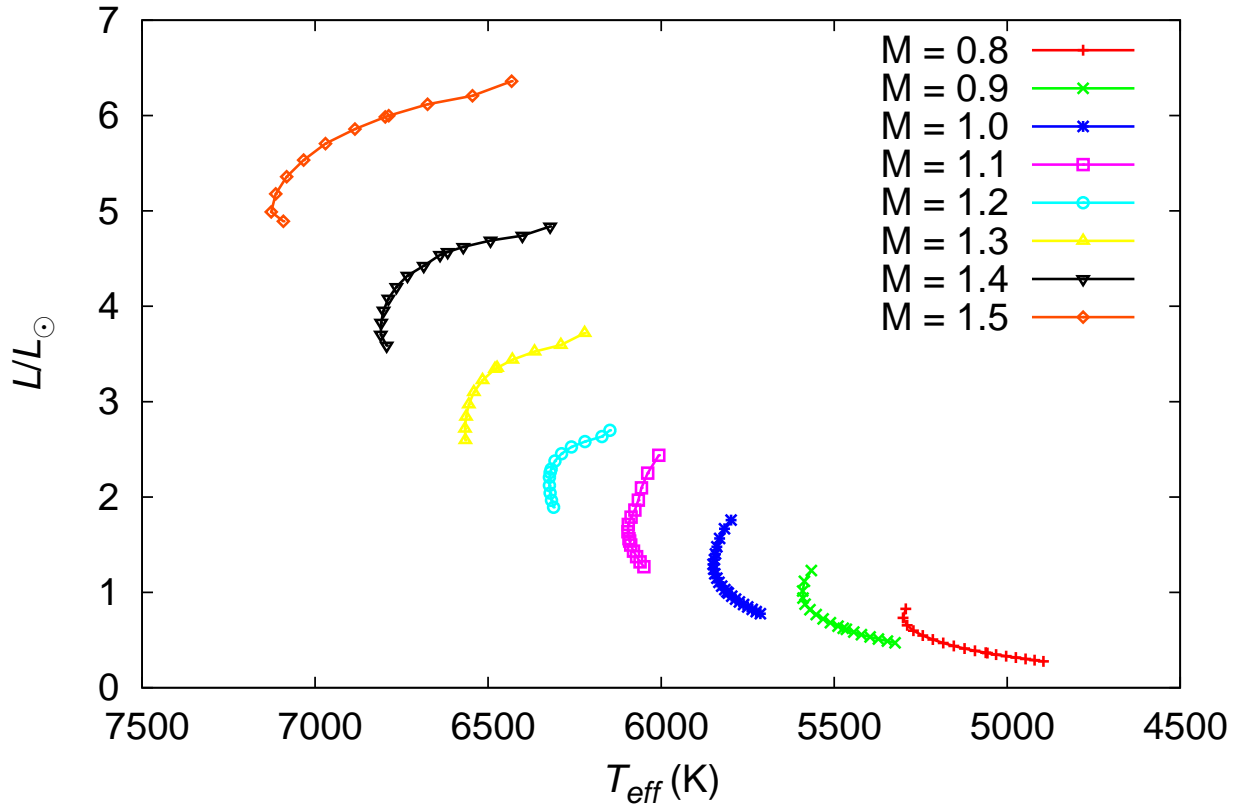


Fig. 2.— H-R diagram showing the evolutionary stages of the models under study.

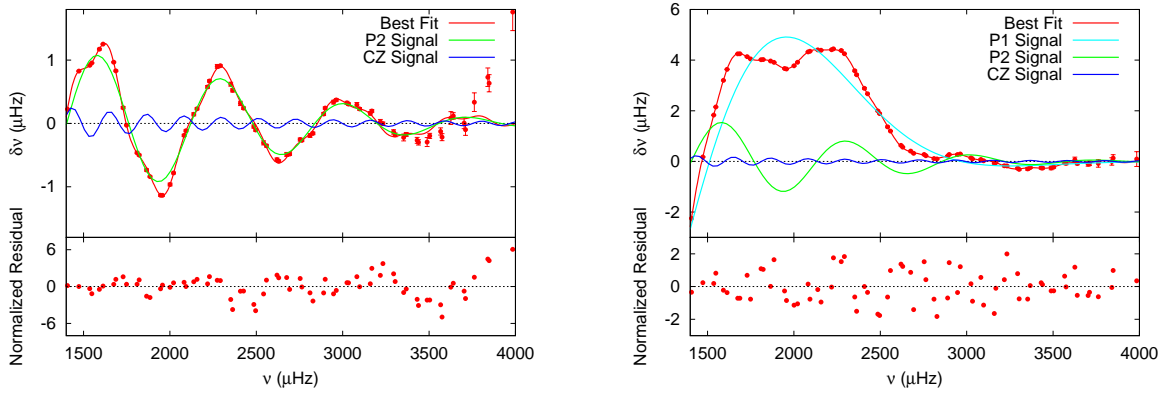


Fig. 3.— The fit to the observed BiSON frequencies using Method A. The figure shows the oscillatory part of the frequency ($\delta\nu$) obtained by subtracting the smooth part from the frequencies. The dots show the observed BiSON frequencies. The left panel shows the oscillatory component of the fit ($\delta\nu$) when only one glitch from He ionization zone is included. The lower panels show the normalized residuals, which are obtained by dividing the residual with the error on the frequency. The right panel shows the fit when the oscillatory signal due to P1 (see Fig. 1) is also included in the fit.

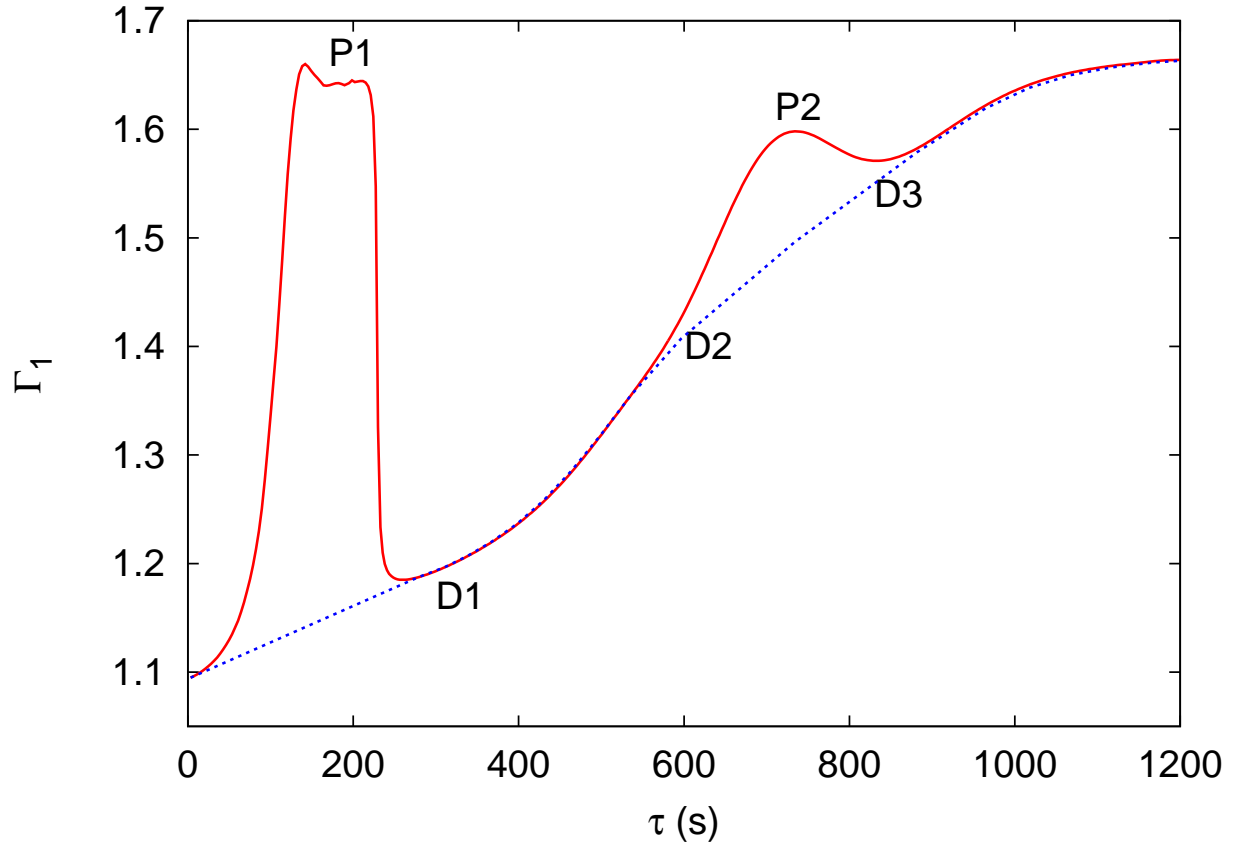


Fig. 4.— The first adiabatic index as a function of acoustic depth of a solar model constructed with a realistic atmosphere. The atmosphere extends to an optical depth of 2×10^{-6} . The dotted line is an eye guide to the Γ_1 profile that contributes to the smooth component of the frequency.

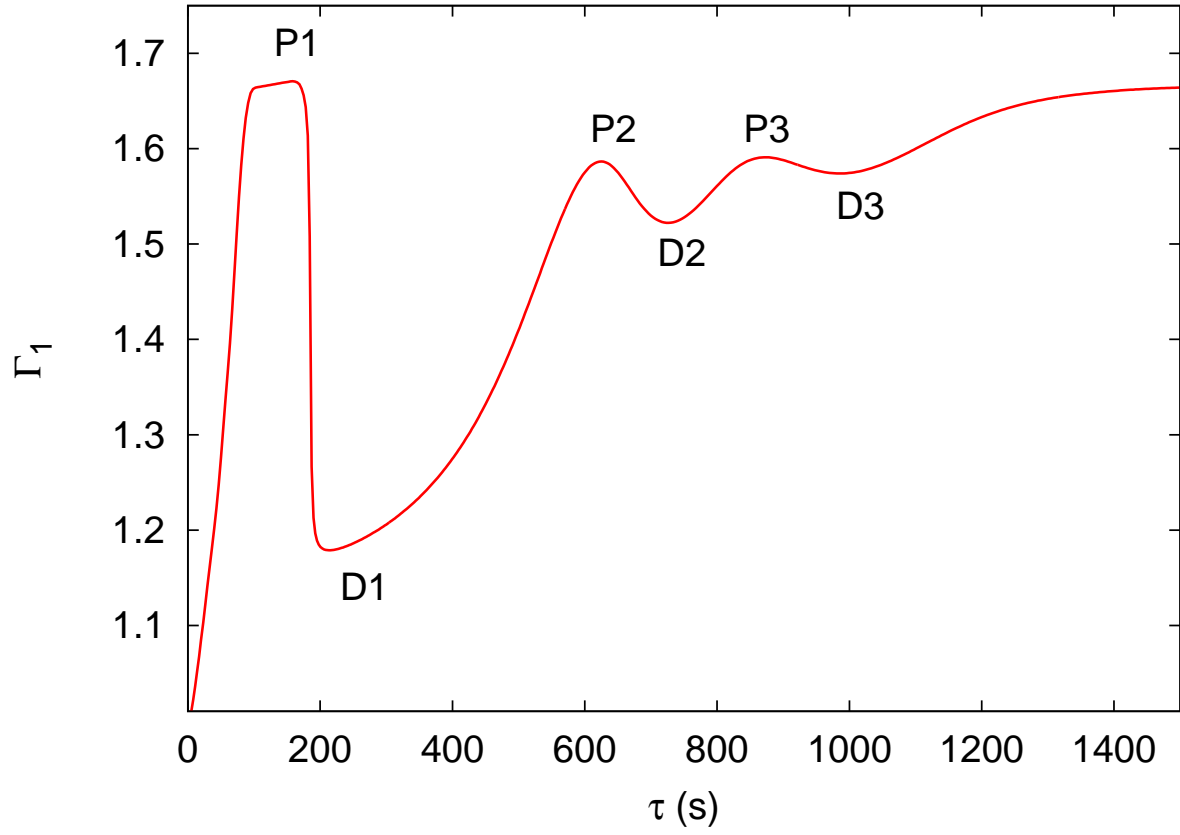


Fig. 5.— The first adiabatic index as a function of acoustic depth for a solar model constructed with increased helium ionization potentials to separate out the HI and HeI ionization zones.

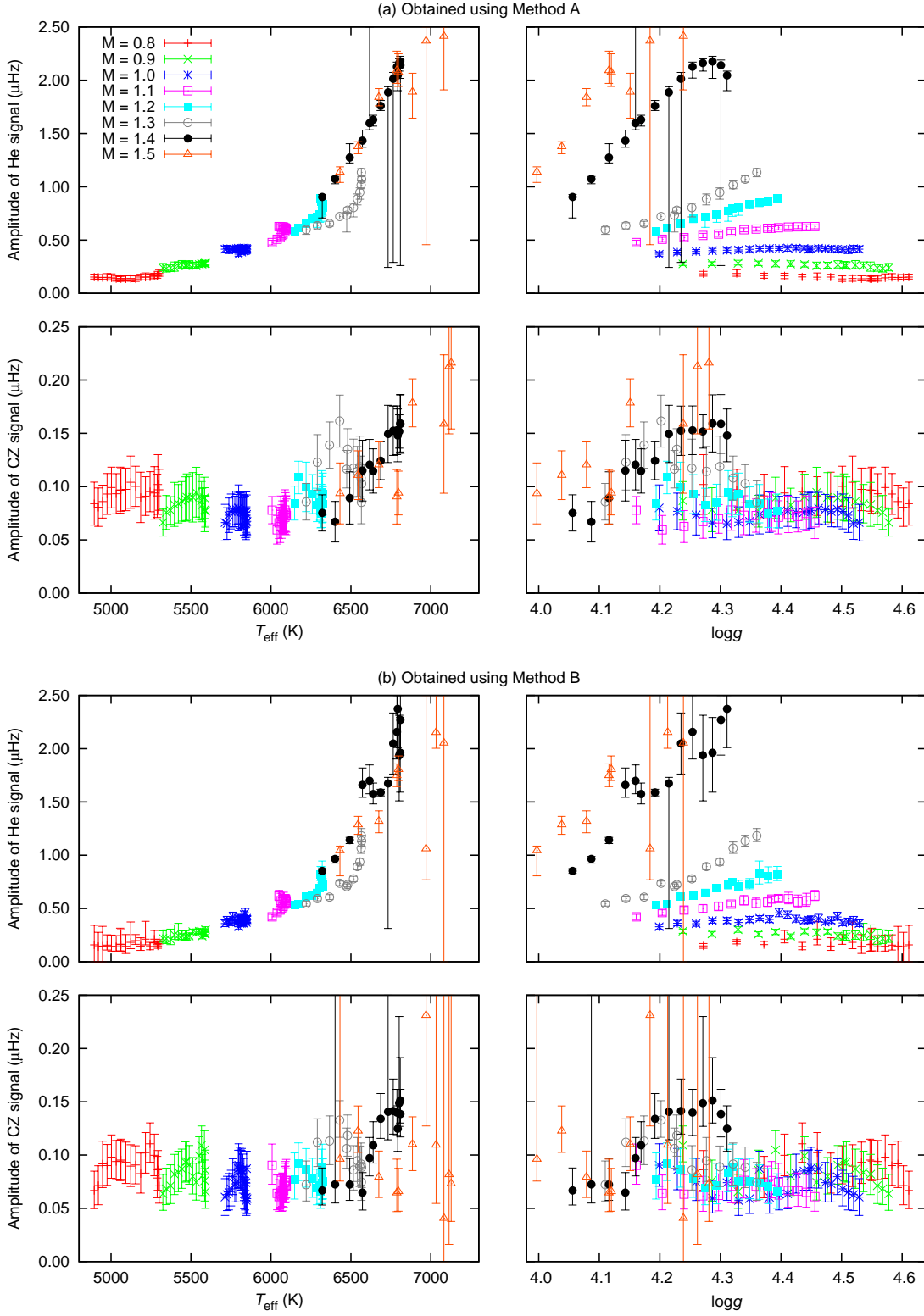


Fig. 6.— The amplitude of He and CZ signal averaged over the frequency interval used in the fit, as a function of the effective temperature and the logarithm of the surface gravity. Different types of points correspond to the masses of the stars as shown in top left panel.

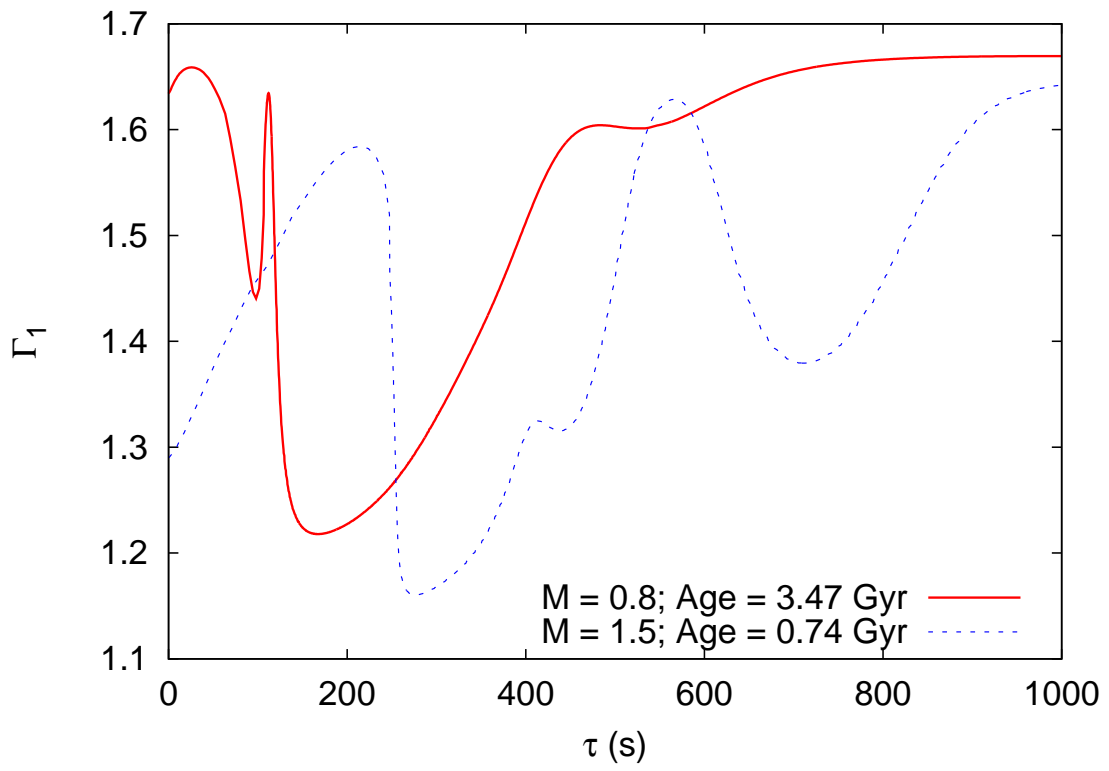


Fig. 7.— The typical profiles of first adiabatic index for models of masses $0.8M_{\odot}$ and $1.5M_{\odot}$.

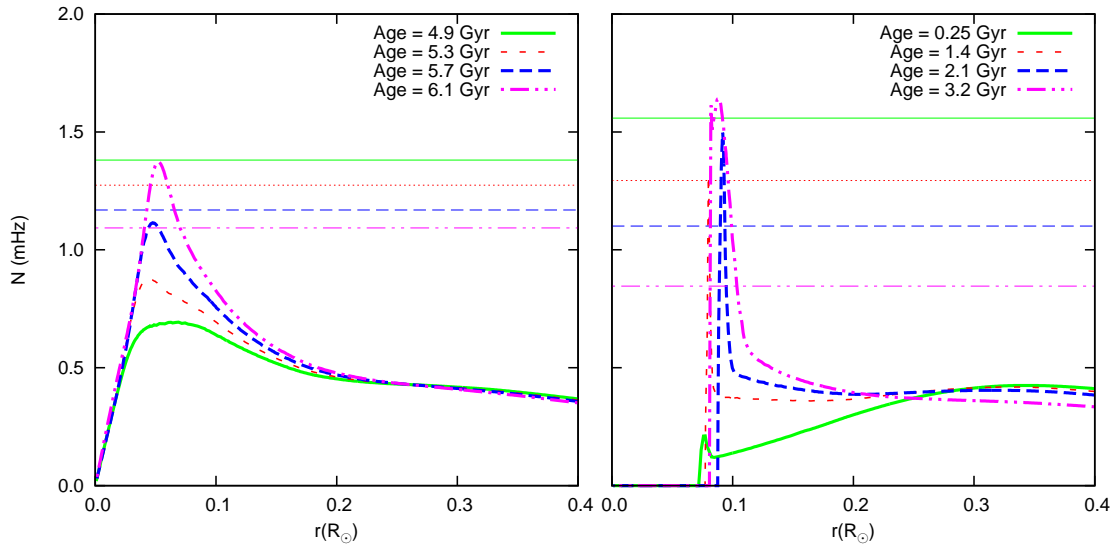


Fig. 8.— The Brunt-Väisälä frequency of selected models of mass $1.1M_{\odot}$ (left panel) and $1.3M_{\odot}$ (right panel) as a function of radial coordinate. The horizontal lines correspond to the lowest frequency used in fitting the signal.

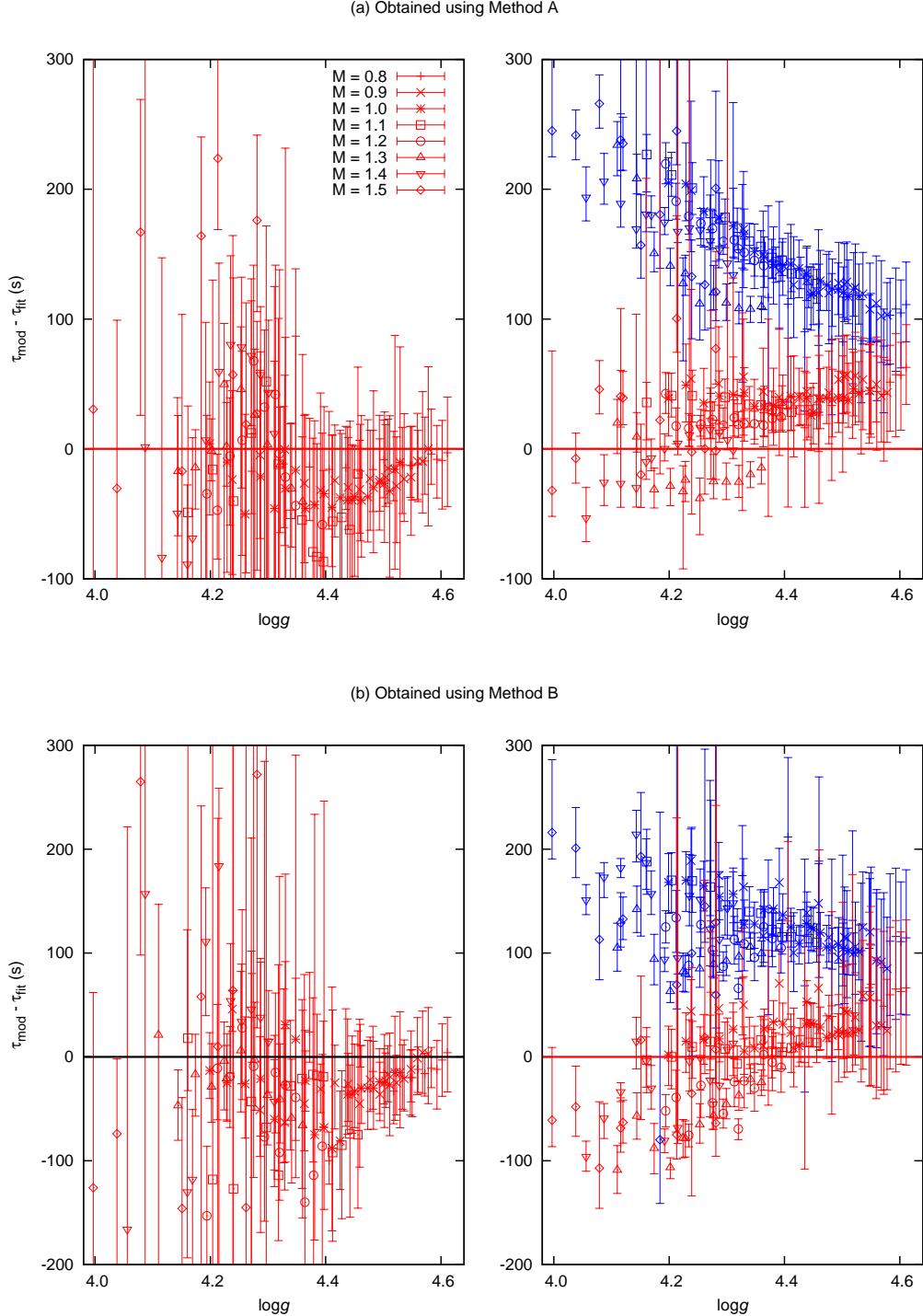


Fig. 9.— The differences between the fitted τ_g and the acoustic depth of various glitches as obtained using sound speed profile. The left panels show the difference between the acoustic depth of the base of convection zone and the fitted τ_{CZ} , while the right panels show the difference $\tau_{P2} - \tau_{He}$ (red points) and $\tau_{D3} - \tau_{He}$ (blue points). Different types of points correspond to the masses of the stars as shown in top left panel.

Table 1. The fitted parameters for the Sun and 16 Cyg A as obtained using Method A and B.

Method	χ^2	A_{CZ} (μHz)	τ_{CZ} (s)	A_{He} (μHz)	Δ_{He} (s)	τ_{He} (s)
Sun						
A	262	0.092 ± 0.002	2320 ± 6	0.594 ± 0.003	60.2 ± 0.3	696 ± 1
B	1080	0.080 ± 0.002	2323 ± 4	0.637 ± 0.004	61.3 ± 0.3	707 ± 1
Solar model						
A	235	0.099 ± 0.002	2296 ± 5	0.590 ± 0.003	61.4 ± 0.3	686 ± 1
B	1124	0.085 ± 0.002	2300 ± 4	0.632 ± 0.004	61.9 ± 0.3	699 ± 1
16 Cyg A						
A	74.4	0.055 ± 0.012	3049 ± 57	0.508 ± 0.017	100.4 ± 3.7	930 ± 13
B	68.9	0.072 ± 0.011	3079 ± 54	0.492 ± 0.013	109.0 ± 7.0	919 ± 9
16 Cyg A model						
A	2.34	0.077 ± 0.015	3096 ± 51	0.506 ± 0.018	95.8 ± 3.6	883 ± 14
B	17.8	0.080 ± 0.012	3098 ± 39	0.492 ± 0.013	113.9 ± 7.8	865 ± 9

Table 2. The fitted parameters for the solar model and the BiSON frequencies using Method A with HeI term.

$\eta = \tau_I/\tau_{II}$	χ^2	A_{CZ} (μHz)	τ_{CZ} (s)	A_I (μHz)	Δ_I (s)	A_{II} (μHz)	Δ_{II} (s)	τ_{II} (s)
Fit to the BiSON Frequencies								
0.90	92.4	0.083 ± 0.002	2331 ± 7	1.023 ± 0.098	90.7 ± 1.0	1.417 ± 0.075	74.7 ± 1.2	631 ± 5
0.80	90.7	0.083 ± 0.002	2331 ± 7	0.659 ± 0.069	89.8 ± 2.6	1.010 ± 0.042	73.3 ± 1.1	648 ± 5
0.70	86.5	0.083 ± 0.002	2330 ± 7	0.540 ± 0.076	89.7 ± 4.1	0.827 ± 0.038	72.1 ± 1.6	660 ± 6
0.60	82.3	0.082 ± 0.002	2331 ± 7	0.562 ± 0.059	90.4 ± 5.2	0.741 ± 0.024	71.4 ± 1.0	668 ± 5
0.50	78.1	0.082 ± 0.002	2331 ± 7	0.704 ± 0.060	90.6 ± 5.0	0.693 ± 0.017	70.6 ± 0.8	675 ± 4
0.40	73.5	0.082 ± 0.002	2330 ± 7	1.060 ± 0.068	89.0 ± 4.6	0.659 ± 0.012	69.9 ± 0.8	680 ± 4
0.30	67.2	0.083 ± 0.002	2329 ± 7	1.964 ± 0.124	84.4 ± 4.2	0.632 ± 0.007	68.8 ± 0.6	686 ± 3
0.25	63.8	0.083 ± 0.002	2328 ± 7	2.970 ± 0.197	81.1 ± 3.6	0.622 ± 0.005	68.0 ± 0.6	689 ± 2
Fit to the Model Frequencies								
0.90	47.9	0.089 ± 0.002	2314 ± 6	1.361 ± 0.129	93.4 ± 1.0	1.669 ± 0.100	77.3 ± 1.0	605 ± 5
0.80	47.5	0.089 ± 0.002	2314 ± 6	0.892 ± 0.092	94.4 ± 2.3	1.155 ± 0.056	75.5 ± 1.0	624 ± 5
0.70	45.4	0.089 ± 0.002	2314 ± 6	0.761 ± 0.069	95.1 ± 3.1	0.933 ± 0.032	74.6 ± 1.0	636 ± 4
0.60	42.8	0.089 ± 0.002	2314 ± 6	0.783 ± 0.071	95.9 ± 3.7	0.816 ± 0.024	73.8 ± 1.0	646 ± 4
0.50	38.6	0.089 ± 0.002	2313 ± 6	0.938 ± 0.076	94.7 ± 4.2	0.742 ± 0.018	73.1 ± 0.8	655 ± 4
0.40	33.2	0.089 ± 0.002	2311 ± 6	1.318 ± 0.082	90.1 ± 4.5	0.685 ± 0.013	72.2 ± 0.8	664 ± 4
0.30	27.3	0.090 ± 0.002	2309 ± 5	2.367 ± 0.139	81.1 ± 3.7	0.639 ± 0.008	70.8 ± 0.6	674 ± 3
0.25	25.6	0.091 ± 0.003	2306 ± 6	3.573 ± 0.403	76.2 ± 5.1	0.624 ± 0.010	69.7 ± 1.1	678 ± 4